SCIENCE CHINA
Information Sciences

• **RESEARCH PAPER** •

Colocated MIMO radar waveform design for angular SRL in the context of hypothesis testing

Yunlei ZHANG[1,2], Li WANG[1], Jinbo WANG[2] & Jun TANG[1*]

[1]*Department of Electronic Engineering , Tsinghua University Beijing* 100084*, China;*
[2]*Institute of Electronic Engineering, Navy University of Engineering, Wuhan* 430033*, China*

Abstract Resolvability is an important performance for radars or other sensors. In this paper, a new solution of multiple-input multiple-output (MIMO) radar waveform design is proposed for improving the angular statistical resolution limit (SRL) performance of two closely spaced targets. Exploring Taylor expansion at the known angular center of two targets and making an orthogonal projection, the original resolution problem can be transformed into a detection one, so the criteria of waveform design for target detection can be applized. We have shown that in the presence of signal-dependent interferences, maximizing the output signal-to-interference-plus-noise ratio (SINR) and maximizing the relative entropy, will resort to the same non-convex model. With the model, we have adopted an existing alternative optimization to design the optimal waveform. Simulations demonstrate that the optimal waveform outperforms the orthogonal and the coherent waveforms in term of the resolution performance in the presence of signal-dependent interferences.

Keywords hypothesis testing, angular resolution, waveform design, colocated MIMO radar, statistical resolution limit

Citation Yunlei ZHANG, Li WANG, Jinbo WANG, et al. Title for citation. Sci China Inf Sci, for review

1 Introduction

Resolution is always an important performance for radars or other sensors [1]. Traditionally, the angular resolution limit is decided by the size of the antenna aperture, named as Rayleigh limit [2]. However, with the advent of high-resolution spectral estimation, it is necessary to measure the super-resolution performance.

The earliest definition of super-resolution was in an observed way. For example, it was pointed out that there would be a hollow between the spectra of two separated signals [3], so the problem was transformed into detecting whether the hollow was existing or not. Later a zero-crossing method based on the second-order characteristics of directional spectrum had been presented [4], which could avoid the error caused by the offset of the estimation directional spectrum. However, these methods regarded the resolution problem as a determined one, not considering the influence of noise and clutter. Thus, some works from the statistical viewpoint, based on the notion of the Cramer-Rao bound (CRB), have been put forward. For example, the larger CRB of parameters of interest (POIs) of two signals was taken as a criterion in [5], further the CRB of the interval of POIs was taken in [6]. In this way, the limit corresponds to a certain probability, reflecting the statistical characteristics of the echo, therefore is called statistical resolution limit (SRL).

* Corresponding author (email: tangj_ee@tsinghua.edu.cn)

Recently, a new definition of the SRL in the context of hypothesis testing, have been widely studied [7–11]. The angular SRL of two point targets in three-dimensional space was deduced in presence of Gaussian white noise [7]. Then the work was extended to the case that the point source interferences were present [8], where the orthogonal projection theory was carried out to eliminate the unknown parameters. In the same way, the angular statistical resolution limit (SRL) of colocated MIMO radar was discussed in [9], and the information theory criterion was applied in [10]. Recently, the general likelihood rate test (GLRT) is extended to Rao detection in [11]. We resolve SRL using a general model with unknown center of the POIs in [12]. These studies have demonstrated that the SRL is related not only to the signal-interference-plus-noise ratio (SINR), but also to the transmitted signal waveforms.

However, no research has been conducted on how to design the waveforms to achieve a better resolution. It is widely known, that MIMO radars allow each array element to transmit different waveforms. The additional degrees of freedom (DOFs) offered by the diversified waveforms can be used to maximize the SINR in the presence of signal-dependent interferences [13]. Up to now, the research of waveform design for MIMO radar mainly includes: the synthesis of the waveforms with the desired beam response [14–16], the maximum of the probability of detection [17–21] and minimizing estimation error [22]. To maximize the detection probability, one widely used criteria is the maximum of SINR [17–19], another is maximizing the relative entropy [20,21]. These two approaches are consistent in some scenarios [23]. In fact, the waveform design of MIMO radar in presence of interference is how to allocate energy spatial distribution [24]. It has been widely accepted that, the phased-array radar has best energy focusing, but its DOFs for the interference suppression are less. On the contrary, the orthogonal MIMO radar has the most DOFs, which can be used for clutter suppression, but the energy transmitted in the target direction is less as it is evenly distributed in the whole space. Therefore, the essence of waveform design is how to balance the performances between the interference suppression and the target detection, which can be achieved by maximizing the output SINR or the information entropy, so these two criteria has been widely used for design standard in the radar detection. However, they cannot be used directly to solve our resolution model, where there are two signals in the echo.

To eliminate the unknown parameters, the projection theory has been brought in [8], which inspired us to design the colocated MIMO radar waveforms for angular resolution. With our Gaussian distribution assumption, we will show that the criteria of maximizing the output SINR and maximizing the information entropy is consistent, and resort to a same model. To solve the unified non-convex model, we employ the existing alternative optimal method. Compared with the orthogonal and coherent waveforms, our optimal waveform can improve the resolution rate for two closely-spaced targets in the presence of signal-dependent interferences.

From the statistical aspect, the SRL is actually related to the resolution rate and the false-alarm rate, the former reflects the probability of correctly resolving two closely-spaced sources, while the latter is the probability of falsely resolving two sources when only one is present. The resolution performance of MIMO radar can be measured in two aspects—one is the minimum interval of two close parameters that can discriminate with a given resolution rate; the other is to maximize the resolution rate with a given interval. According, the waveform design for resolution can also be divided into two approaches—one is to minimize the resolution limit with a given probability; the other is to maximize the resolution rate with a given separation of the two POIs. In fact, the two methods are same, and we will focus on the latter one in this study.

The rest of our paper is arranged as follows: Section 2 presents the model of our resolution problem, and Section 3 shows the consistency of the two criteria for our model. In Section 4 we present an alternative optimal algorithm to solve the non-convex model, whose performance is simulated in Section 5. Finally Section 6 concludes our paper.

2 Resolution Model

The sketch of the colocated MIMO radar is shown in Figure 1, where a far-field and narrow-band signal model is assumed. To point out that, the degrees of arrival(DOA) and departure(DOD) are same for colocated MIMO radar. However, for easy comprehension we plot a bi-static sketch here. We assume that the DOAs of two targets are nearly the same. The MIMO radar has N_t transmitting elements and N_r receiving elements, while the former has an interval of N_r times of half wavelength and the latter a half wavelength. Take the first element as the phase reference, and then the transmit and receive array

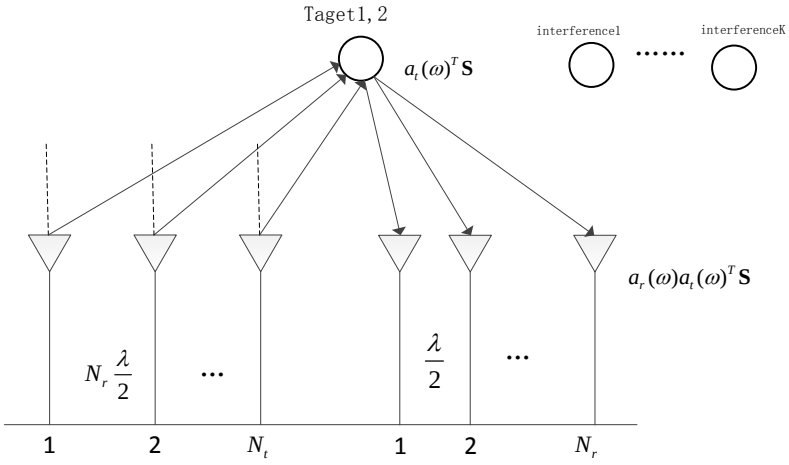

Figure 1 Sketch of colocated MIMO radar.

steering vector can be expressed as

$$\begin{cases} \boldsymbol{a}_t(\omega_p) = [1, e^{-jN_r\omega_p}, e^{-2jN_r\omega_p}, \cdots, e^{-(N_t-1)jN_r\omega_p}]^T \\ \boldsymbol{a}_r(\omega_p) = [1, e^{-j\omega_p}, e^{-2j\omega_p}, \cdots, e^{-(N_r-1)j\omega_p}]^T \end{cases}, \tag{1}$$

where $\omega_p = \pi sin\theta_p, p = 1, 2$, denoting the angular frequency of two targets. The superscript $()^T$ is the transpose of a matrix or a vector.

Denote the transmitted signals $\boldsymbol{S} \in \mathbb{C}^{N_t \times L}$ as $\boldsymbol{S} = [s_1, s_2, \ldots, s_{N_t}]^T$, where $s_n \in \mathbb{C}^{L\times 1}, n = 1 : N$ is a L-length complex signal transmitted by the n-th element, L is the sampling number. It should be paid attention that, the signals transmitted by different elements may not be orthogonal with each other. On the contrary, we aim to design these non-orthogonal signals to yield the best performance. Not considering the propagation attenuation, the collection of the transmitted signals at the spot of target with w_p angle frequency can be written as $\boldsymbol{a}_t(\omega_p)^T\boldsymbol{S}$. The signals reflected by the targets then received by the array, which is $\alpha_p\boldsymbol{a}_r(\omega_p)\boldsymbol{a}_t(\omega_p)^T\boldsymbol{S}$, where α_p is the complex response of the p-th target, reflecting the two-round attenuation and its radar cross section(RCS).

We consider K signal-dependent point interferences, and denote β_k as the response of the k-th interference, and ω_k and n_k are the angular frequency and the range cells occupied by the k-th interference, respectively. Similarly, the interference signals in the echo can be presented as $\beta_k\boldsymbol{a}_r(\omega_k)\boldsymbol{a}_t(\omega_k)^T\boldsymbol{S}\boldsymbol{J}_{n_k}$,where $\boldsymbol{J}_{n_k}$ is the shifting matrix, with ones on the n_k-th diagonal and zeros elsewhere. Then the echo matrix of all the receiving elements can be expressed as

$$\boldsymbol{Y} = \sum_{p=1}^{2}\alpha_p\boldsymbol{a}_r(\omega_p)\boldsymbol{a}_t(\omega_p)^T\boldsymbol{S} + \sum_{k=1}^{K}\beta_k\boldsymbol{a}_r(\omega_k)\boldsymbol{a}_t(\omega_k)^T\boldsymbol{S}\boldsymbol{J}_{n_k} + \boldsymbol{N}, \tag{2}$$

where $\boldsymbol{Y}, \boldsymbol{N} \in \mathbb{C}^{N_r\times L}$, the latter is the noise matrix [18].

With the transformation $vec(\boldsymbol{ABC}) = (\boldsymbol{C}^T \otimes \boldsymbol{A})vec(\boldsymbol{B})$, where $\otimes$ is the operation of Kronecker product, $vec()$ is the vectorization of a matrix by stacking all its column vectors. Let $\boldsymbol{y} = vec(\boldsymbol{Y})$,$\boldsymbol{n} = vec(\boldsymbol{N})$,$\boldsymbol{s} = vec(\boldsymbol{S}) \in \mathbb{C}^{N_t L \times 1}$, the echo matrix can be converted into a vector as

$$\boldsymbol{y} = \sum_{p=1}^{2} \alpha_p \boldsymbol{A}_p \boldsymbol{s} + \sum_{k=1}^{K} \beta_k \boldsymbol{B}_k \boldsymbol{s} + \boldsymbol{n}, \tag{3}$$

where $\boldsymbol{A}_p = \boldsymbol{I}_L \otimes \left(\boldsymbol{a}_r(\omega_p)\boldsymbol{a}_t(\omega_p)^T\right)$ and $\boldsymbol{B}_k = \boldsymbol{J}_{n_k} \otimes \left(\boldsymbol{a}_r(\omega_k)\boldsymbol{a}_t(\omega_k)^T\right)$.

Here we assume that the separation of two signals, i.e., $\delta_\omega = \omega_2 - \omega_1$, are very small, and the center value of POIs is $\omega_0 = (\omega_1 + \omega_2)/2$, is assumed to be known as a *priori*. Therefore we can make the first-order Taylor expansion at ω_0, and reserve it as the approximation of the two signals, so we obtain

$$\boldsymbol{y} \approx (\alpha_1 + \alpha_2)\boldsymbol{A}_0 \boldsymbol{s} + (\alpha_1 - \alpha_2)\frac{\delta_\omega}{2}\dot{\boldsymbol{A}}_0 \boldsymbol{s} + \sum_{k=1}^{K} \beta_k \boldsymbol{B}_k \boldsymbol{s} + \boldsymbol{n}, \tag{4}$$

where $\boldsymbol{A}_0 = \boldsymbol{I}_L \otimes (\boldsymbol{a}_r(\omega_0)\boldsymbol{a}_t(\omega_0)^T)$, $\dot{\boldsymbol{A}}_0 = \boldsymbol{I}_L \otimes \left(\dot{\boldsymbol{a}}_r(\omega_0)\boldsymbol{a}_t(\omega_0)^T\right) + \boldsymbol{I}_L \otimes \left(\boldsymbol{a}_r(\omega_0)\dot{\boldsymbol{a}}_t(\omega_0)^T\right)$ is the first-order derivation of $\boldsymbol{A}_0$ at ω_0. $\dot{\boldsymbol{a}}_t(\omega_0), \dot{\boldsymbol{a}}_r(\omega_0)$ are the first-order derivation of $\boldsymbol{a}_t(\omega_0)$ and $\boldsymbol{a}_r(\omega_0)$ at ω_0.

As previously stated, we use the orthogonal projection to convert the original resolution model into a detection one. Matrix $\boldsymbol{A}_0$ is not column-full-rank, so we take these uncorrelated columns of the matrix to compose a new matrix $\boldsymbol{X}$. Then the projection matrix on the subspace spanned by the columns of the matrix $\boldsymbol{A}_0$, can be expressed as

$$P_{\boldsymbol{A}_0}^{\perp} = \boldsymbol{I}_{N_r L} - \boldsymbol{X}(\boldsymbol{X}^H \boldsymbol{X})^{-1}\boldsymbol{X}^H, \tag{5}$$

where the superscript $()^H$ denotes the conjugation and transpose of a matrix or vector, the superscript $()^{\perp}$ is the orthogonal projector. As $rank\{\boldsymbol{A}_0\} = L$, there is $rank\{\boldsymbol{P}_{\boldsymbol{A}_0}^{\perp}\} = (N_r - 1)L \triangleq Q$. Make the orthogonal decomposition as $P_{\boldsymbol{A}_0}^{\perp} = \boldsymbol{U}\boldsymbol{U}^H$, which meets $\boldsymbol{U}^H\boldsymbol{U} = \boldsymbol{I}_Q$. Let $\tilde{\boldsymbol{y}} = \boldsymbol{U}^H\boldsymbol{y}$ and $\tilde{n} = \boldsymbol{U}^H\boldsymbol{n}$. Multiplying $\boldsymbol{U}^H$ to the two sides of (4), we get a detection model as

$$\tilde{\boldsymbol{y}} = (\alpha_1 - \alpha_2)\frac{\delta_\omega}{2}\boldsymbol{U}^H\dot{\boldsymbol{A}}_0\boldsymbol{s} + \sum_{k=1}^{K}\beta_k\boldsymbol{U}^H\boldsymbol{B}_k\boldsymbol{s} + \tilde{\boldsymbol{n}}. \tag{6}$$

Let $\boldsymbol{t} = \boldsymbol{H}\theta$, where $\boldsymbol{H} = \boldsymbol{U}^H\dot{\boldsymbol{A}}_0\boldsymbol{s}$, $\theta = (\alpha_1 - \alpha_2)\frac{\delta_\omega}{2}$, $\boldsymbol{c} = \sum_{k=1}^{K}\beta_k\boldsymbol{U}^H\boldsymbol{B}_k\boldsymbol{s}$, a binary hypothesis model can be established as

$$\tilde{\boldsymbol{y}} = \begin{cases} \boldsymbol{c} + \tilde{\boldsymbol{n}}, H_0 \\ \boldsymbol{t} + \boldsymbol{c} + \tilde{\boldsymbol{n}}, H_1 \end{cases}. \tag{7}$$

We should decide whether hypotheses H_0 or H_1 is true. For H_0, there is $\theta = 0$, denoting only one target is present; while for H_1, there is $\theta \neq 0$, denoting there are two targets.

Assuming that each target, each interference and noise are independent with each other, obeying to Gaussian distribution, i.e.,$\alpha_p \sim \mathcal{CN}(0, \sigma_p^2), p = 1, 2$, so there is

$$\boldsymbol{R}_t = E\{\boldsymbol{t}\boldsymbol{t}^H\} = (\sigma_1^2 + \sigma_2^2)\frac{\delta_\omega^2}{4}\boldsymbol{U}^H\dot{\boldsymbol{A}}_0\boldsymbol{s}\boldsymbol{s}^H\dot{\boldsymbol{A}}_0^H\boldsymbol{U}, \tag{8}$$

where $E\{\}$ denotes the operation of expectation. While for the interferences, there is $\beta_k \sim \mathcal{CN}(0, \sigma_{c,k}^2), k = 1:K$, so the covariance matrix of interferences is $\boldsymbol{R}_c = E\{\boldsymbol{c}\boldsymbol{c}^H\} = \sum_{k=1}^{K}\sigma_{c,k}^2\boldsymbol{U}^H\boldsymbol{B}_k\boldsymbol{s}\boldsymbol{s}^H\boldsymbol{B}_k^H\boldsymbol{U}$. The noise will remain white after project transformation, as there is $\boldsymbol{R}_n = E\{\tilde{\boldsymbol{n}}\tilde{\boldsymbol{n}}^H\} = \boldsymbol{U}^H E\{\boldsymbol{w}\boldsymbol{w}^H\}\boldsymbol{U} = \sigma_n^2\boldsymbol{I}_Q$. Therefore the covariance matrix of the noise and interference is

$$\boldsymbol{R}_{nc} = \boldsymbol{R}_c + \boldsymbol{R}_n = \sum_{k=1}^{K}\sigma_{c,k}^2\boldsymbol{U}^H\boldsymbol{B}_k\boldsymbol{s}\boldsymbol{s}^H\boldsymbol{B}_k^H\boldsymbol{U} + \sigma_n^2\boldsymbol{I}_Q. \tag{9}$$

Therefore we can get the distributions of $\tilde{\boldsymbol{y}}$ under two hypotheses as

$$\tilde{\boldsymbol{y}} \sim \begin{cases} \mathcal{CN}\big(\boldsymbol{0}, \boldsymbol{R}_{nc}\big), H_0 \\ \mathcal{CN}\big(\boldsymbol{0}, \boldsymbol{R}_t + \boldsymbol{R}_{nc}\big), H_1 \end{cases}. \tag{10}$$

Then one can see that, with our assumptions, the echoes under both hypotheses are Gaussian distributions, with different variance matrices.

3 Waveform Design Criteria

According to (10), the probability density functions (PDFs) under two hypotheses are

$$\begin{cases} p_0(\tilde{\boldsymbol{y}}) = \frac{1}{\pi^Q |\boldsymbol{R}_{nc}|} e^{-\tilde{\boldsymbol{y}}^H \boldsymbol{R}_{nc}^{-1} \tilde{\boldsymbol{y}}}, H_0 \\ p_1(\tilde{\boldsymbol{y}}) = \frac{1}{\pi^Q |\boldsymbol{R}_t + \boldsymbol{R}_{nc}|} e^{-\tilde{\boldsymbol{y}}^H (\boldsymbol{R}_t + \boldsymbol{R}_{nc})^{-1} \tilde{\boldsymbol{y}}}, H_1 \end{cases}. \tag{11}$$

As a result, we can rsolve the likelihood rate test. Here we will bring two existing criteria to resolve it.

3.1 Maximum of SINR

According to the distributions in (11), the likelihood rate function can be expressed as

$$\begin{aligned} lnLRT(\tilde{\boldsymbol{y}}) =& lnp_1(\tilde{\boldsymbol{y}}) - lnp_0(\tilde{\boldsymbol{y}}) \\ =& ln|\boldsymbol{R}_{nc}| + \tilde{\boldsymbol{y}}^H \boldsymbol{R}_{nc}^{-1} \tilde{\boldsymbol{y}} \\ & - ln|\boldsymbol{R}_t + \boldsymbol{R}_{nc}| - \tilde{\boldsymbol{y}}^H (\boldsymbol{R}_t + \boldsymbol{R}_{nc})^{-1} \tilde{\boldsymbol{y}}. \end{aligned} \tag{12}$$

Omitting these items unrelated to the data, we get a new statistic as

$$T(\tilde{\boldsymbol{y}}) = \tilde{\boldsymbol{y}}^H \big(\boldsymbol{R}_{nc}^{-1} - (\boldsymbol{R}_t + \boldsymbol{R}_{nc})^{-1}\big) \tilde{\boldsymbol{y}}. \tag{13}$$

As $\boldsymbol{R}_\epsilon \triangleq \boldsymbol{R}_{nc}^{-1} - (\boldsymbol{R}_t + \boldsymbol{R}_{nc})^{-1}$ is Hermite and positive semidefinite, we can get its Cholesky factorization as $\boldsymbol{R}_\epsilon = \boldsymbol{T}\boldsymbol{T}^H$. Let $\overline{\boldsymbol{y}} = \boldsymbol{T}^H \tilde{\boldsymbol{y}}$, we can get the distribution of $\overline{\boldsymbol{y}}$ as

$$\overline{\boldsymbol{y}} \sim \begin{cases} \eta_0^2 \chi_{2P}^2, H_0 \\ \eta_1^2 \chi_{2P}^2, H_1 \end{cases}, \tag{14}$$

where $\eta_0^2 = tr\big(\boldsymbol{I}_P - \boldsymbol{R}_{nc}(\boldsymbol{R}_t + \boldsymbol{R}_{nc})^{-1}\big)$ and $\eta_1^2 = tr\big(\boldsymbol{R}_{nc}^{-1}(\boldsymbol{R}_t + \boldsymbol{R}_{nc}) - \boldsymbol{I}_P\big) = tr(\boldsymbol{R}_{nc}^{-1}\boldsymbol{R}_t)$.

As $rank\{\boldsymbol{R}_t\} = 1$ (8), there is decomposition $\boldsymbol{R}_t = \boldsymbol{v}\boldsymbol{v}^H$, where

$$\boldsymbol{v} = (\sigma_1^2 + \sigma_2^2)^{1/2} \boldsymbol{U}^H \dot{\boldsymbol{A}}_0 \boldsymbol{s}. \tag{15}$$

With the matrix inverse lemma $(\boldsymbol{A} + \boldsymbol{B}\boldsymbol{C}\boldsymbol{D})^{-1} = \boldsymbol{A}^{-1} - \boldsymbol{A}^{-1}\boldsymbol{B}(\boldsymbol{C}^{-1} + \boldsymbol{D}\boldsymbol{A}^{-1}\boldsymbol{B})^{-1}\boldsymbol{D}\boldsymbol{A}^{-1}$, η_0^2 can be expressed further as

$$\begin{aligned} \eta_0^2 =& tr\big(\boldsymbol{I}_Q - \boldsymbol{R}_{nc}(\boldsymbol{v}\boldsymbol{v}^H + \boldsymbol{R}_{nc})^{-1}\big) \\ =& tr\big(\boldsymbol{I}_Q - \boldsymbol{R}_{nc}(\boldsymbol{R}_{nc}^{-1} - \boldsymbol{R}_{nc}^{-1}\boldsymbol{v}(\boldsymbol{I}_2 + \boldsymbol{v}^H \boldsymbol{R}_{nc}^{-1}\boldsymbol{v})^{-1}\boldsymbol{v}^H \boldsymbol{R}_{nc}^{-1})\big) \\ =& (1 + \boldsymbol{v}^H \boldsymbol{R}_{nc}^{-1}\boldsymbol{v})^{-1} tr(\boldsymbol{R}_{nc}^{-1}\boldsymbol{R}_t). \end{aligned} \tag{16}$$

From (14), the false-alarm rate p_f can be expressed as

$$\begin{aligned} p_f =& P(T(\tilde{y}) > \gamma | H_0) \\ =& P(\eta_0^2 \chi_{2Q}^2 > \gamma) = P(\chi_{2Q}^2 > \gamma/\eta_0^2). \end{aligned} \tag{17}$$

With the given p_f, the threshold can be got as $\gamma = \eta_0^2 Q_{\chi_{2P}^2}^{-1}(p_f)$, where $Q_{\chi_{2Q}^2}^{-1}()$ is the inverse function of $Q_{\chi_{2Q}^2}()$, which is the the right-tail function of Chi-Square distribution with $2Q$ degrees.

Similarly, the detection rate p_d can be expressed as

$$\begin{aligned} p_d =& P(T(\tilde{y}) > \gamma | H_1) \\ =& P(\eta_1^2 \chi_{2Q}^2 > \gamma) = P(\chi_{2Q}^2 > \gamma/\eta_1^2) \\ =& Q_{\chi_{2Q}^2}\big(\eta_0^2/\eta_1^2 Q_{\chi_{2Q}^2}^{-1}(p_f)\big), \end{aligned} \tag{18}$$

which is actually the resolution probability of original model.

From (18), one can see the resolution rate is monotonically decreasing with η_0^2/η_1^2, so maximizing the resolution rate is equivalent to

$$\begin{aligned} max_{\boldsymbol{s}} \eta_1^2/\eta_0^2 &= max_{\boldsymbol{s}}(1 + \boldsymbol{v}^H \boldsymbol{R}_{nc}^{-1} \boldsymbol{v}) \\ &\leftrightarrow max_{\boldsymbol{s}} \boldsymbol{v}^H \boldsymbol{R}_{nc}^{-1} \boldsymbol{v} \\ &\leftrightarrow max_{\boldsymbol{s}} \boldsymbol{s}^H \dot{\boldsymbol{A}}_0^H \boldsymbol{U} \boldsymbol{R}_{nc}^{-1} \boldsymbol{U}^H \dot{\boldsymbol{A}}_0 \boldsymbol{s}. \end{aligned} \tag{19}$$

where the second to last item is just the expression of output SINR, as $\boldsymbol{v}^H \boldsymbol{R}_{nc}^{-1} \boldsymbol{v} = \boldsymbol{R}_{nc}^{-1} \boldsymbol{R}_t$, where $\boldsymbol{R}_{nc}$ and $\boldsymbol{R}_t$ denote the power of the noise-plus-interference and signals, respectively. Therefore maximizing the output SINR is widely accepted as a criteria.

With the constraint of transmitting energy, we establish an optimal problem via (19) as

$$P_1 \begin{cases} argmax_{\boldsymbol{s}} \;\; \boldsymbol{s}^H \dot{\boldsymbol{A}}_0^H \boldsymbol{U} \boldsymbol{R}_{nc}^{-1}(\boldsymbol{s}) \boldsymbol{U}^H \dot{\boldsymbol{A}}_0 \boldsymbol{s} \\ s.t. \qquad\quad \boldsymbol{s}^H \boldsymbol{s} \leqslant p_t \end{cases}, \tag{20}$$

where one can see that, the waveform $\boldsymbol{s}$ is in the inverse of $\boldsymbol{R}_{nc}$, which makes it non-convex and cannot be resolved directly. Then we have to find out the efficient solution, which will be presented in Section 4.

3.2 Maximum of KL divergence

On the other hand, the waveform design has also been discussed to maximize KL divergence in [22]. This is based on the Stein lemma, which describes the relations of the probability of detection p_d and KL divergence $D(p_0||p_1)$ under the given probability of the false-alarm, as

$$D(p_0||p_1) = \lim_{N\to\infty} \big(-\frac{1}{N} log(1 - p_d) \big), \tag{21}$$

where N is the dimension of the random variable.

According to (11), we can obtain the expression of the KL divergence by inserting the two distribution under different hypothesis, as

$$\begin{aligned} D(p_0||p_1) =& \int p_0(\tilde{\boldsymbol{y}}) log \frac{p_0(\tilde{\boldsymbol{y}})}{p_1(\tilde{\boldsymbol{y}})} d\tilde{\boldsymbol{y}} \\ =& logdet(\boldsymbol{R}_t + \boldsymbol{R}_{nc}) - logdet(\boldsymbol{R}_{nc}) \\ &+ tr\big((\boldsymbol{R}_t + \boldsymbol{R}_{nc})^{-1} \boldsymbol{R}_{nc}\big) - Q, \end{aligned} \tag{22}$$

where $det()$ denotes the determinant operator.

With the decomposition $R_t = \boldsymbol{v}\boldsymbol{v}^H$, and the fact that $\boldsymbol{R}_{nc}$ is positive semidefinite, the KL divergence can be further expressed as

$$\begin{aligned} D(p_0||p_1) =& logdet(\boldsymbol{v}\boldsymbol{v}^H + \boldsymbol{R}_{nc}) - logdet(\boldsymbol{R}_{nc}) \\ &+ tr\big((\boldsymbol{v}\boldsymbol{v}^H + \boldsymbol{R}_{nc})^{-1} \boldsymbol{R}_{nc}\big) - Q \\ =& logdet(\boldsymbol{R}_{nc}^{-1/2} \boldsymbol{v}\boldsymbol{v}^H \boldsymbol{R}_{nc}^{-1/2} + \boldsymbol{I}_Q) \\ &+ tr\big(\boldsymbol{R}_{nc}^{-1/2} \boldsymbol{v}\boldsymbol{v}^H \boldsymbol{R}_{nc}^{-1/2} + \boldsymbol{I}_Q)^{-1}\big) - Q, \end{aligned} \tag{23}$$

where the first item is equal to $logdet(\boldsymbol{v}^H \boldsymbol{R}_{nc}^{-1} \boldsymbol{v} + 1) + Q - 1$ [21], and the second item is equal to $tr\big((\boldsymbol{v}^H \boldsymbol{R}_{nc}^{-1} \boldsymbol{v} + 1)^{-1}\big)$ [25]. Therefore we obtain $D(p_0||p_1) = log(1+m) + (1+m)^{-1} - 1$, where $m = \boldsymbol{v}^H \boldsymbol{R}_{nc}^{-1} \boldsymbol{v}$.

It is obvious that $D(p_0||p_1)$ is a monotonous function when $m > 0$ [22], after inserting the expression of $\boldsymbol{v}$ in (27), the maximum of the KL divergence can be recast as

$$\max_{\boldsymbol{s}} \boldsymbol{v}^H \boldsymbol{R}_{nc}^{-1} \boldsymbol{v} \leftrightarrow \max_{\boldsymbol{s}} \boldsymbol{s}^H \dot{\boldsymbol{A}}_0^H \boldsymbol{U} \boldsymbol{R}_{nc}^{-1}(\boldsymbol{s}) \boldsymbol{U}^H \dot{\boldsymbol{A}}_0 \boldsymbol{s}. \tag{24}$$

Therefore, the optimal problem is be equitant to the P_2 in (26).

4 Alternate Optimization Algorithm

As for the non-convex model in (26) in above Section, we present an alternate optimization algorithm. The algorithm is firstly improved in [17], which tackles the model by solving the $\boldsymbol{s}$ and $\boldsymbol{w}$ alternatively, as follows:

Denote by the filter coefficient $\boldsymbol{w} \in \mathbb{C}^{Q\times 1}$, and then the expression of output SINR via (6) is

$$\text{SINR} = \frac{(\sigma_1^2 + \sigma_2^2)\delta_\omega^2}{4} \frac{\boldsymbol{w}^H \boldsymbol{U}^H \dot{\boldsymbol{A}}_0 \boldsymbol{s} \boldsymbol{s}^H \dot{\boldsymbol{A}}_0^H \boldsymbol{U} \boldsymbol{w}}{\boldsymbol{w}^H \boldsymbol{R}_{nc} \boldsymbol{w}}, \tag{25}$$

where the optimal filter is the minimum variance distortionless response (MVDR) filter, which can keep the signal non-variant but minimize the output of the interference and noise, respecting that

$$P_2 \begin{cases} argmin_{\boldsymbol{w}} & \boldsymbol{w}^H \boldsymbol{R}_{nc} \boldsymbol{w} \\ s.t. & \boldsymbol{w}^H \boldsymbol{U}^H \dot{\boldsymbol{A}}_0 \boldsymbol{s} = 1 \end{cases}. \tag{26}$$

Resolving P_1, the MVDR filter can be expressed as

$$\boldsymbol{w} = \frac{\boldsymbol{R}_{nc}^{-1} \boldsymbol{U}^H \dot{\boldsymbol{A}}_0 \boldsymbol{s}}{\boldsymbol{s}^H \dot{\boldsymbol{A}}_0^H \boldsymbol{U} \boldsymbol{R}_{nc}^{-1} \boldsymbol{U}^H \dot{\boldsymbol{A}}_0 \boldsymbol{s}}. \tag{27}$$

By plugging the expression of $\boldsymbol{w}$ into (25), we obtain the SINR which is only related to the signal $\boldsymbol{s}$ as

$$\text{SINR} = \frac{(\sigma_1^2 + \sigma_2^2)\delta_\omega^2}{4} \boldsymbol{s}^H \dot{\boldsymbol{A}}_0^H \boldsymbol{U} \boldsymbol{R}_{nc}^{-1}(\boldsymbol{s}) \boldsymbol{U}^H \dot{\boldsymbol{A}}_0 \boldsymbol{s}, \tag{28}$$

With some transformations, the SINR in (25) can be rewritten as

$$\text{SINR} = \frac{(\sigma_1^2 + \sigma_2^2)\delta_\omega^2}{4} \frac{\boldsymbol{s}^H \dot{\boldsymbol{A}}_0^H \boldsymbol{U} \boldsymbol{w} \boldsymbol{w}^H \boldsymbol{U}^H \dot{\boldsymbol{A}}_0 \boldsymbol{s}}{\boldsymbol{s}^H \boldsymbol{R}_{nc}^{'} \boldsymbol{s}}, \tag{29}$$

where $\boldsymbol{R}_{nc}^{'} \triangleq \sum_{k=1}^{K} \sigma_{c,k}^2 \boldsymbol{B}_k^H \boldsymbol{U} \boldsymbol{w} \boldsymbol{w}^H \boldsymbol{U}^H \boldsymbol{B}_k + \frac{\sigma_n^2}{p_t} \boldsymbol{w}^H \boldsymbol{w} \boldsymbol{I}_{N_t L}$. Then for fixed $\boldsymbol{w}$, the optimal $\boldsymbol{s}$ can be got as

$$P_3 \begin{cases} argmin_{\boldsymbol{s}} & \boldsymbol{s}^H \boldsymbol{R}_{nc}^{'} \boldsymbol{s} \\ s.t. & \boldsymbol{s}^H \dot{\boldsymbol{A}}_0^H \boldsymbol{U} \boldsymbol{w} = K_1 \end{cases}, \tag{30}$$

where K_1 is a constant to guarantee the constraint of the power. The solution of the minimum problem is similar with P_1 in (20), which is $\boldsymbol{s}_1 = \gamma(\boldsymbol{R}_{nc}^{'})^{-1} \dot{\boldsymbol{A}}_0 \boldsymbol{U}^H \boldsymbol{w}$, where γ is a constant to meet the constraint of energy. Then the optimal waveform can be obtained as

$$\boldsymbol{s} = \sqrt{p_t} \boldsymbol{s}_1 / ||\boldsymbol{s}_1||. \tag{31}$$

By solving the optimal $\boldsymbol{s}$ and $\boldsymbol{w}$ alternatively, the optimal solution of (26) can be achieved.

The AOA algorithm is presented in algorithm 1. Denoted the cyclic time of the algorithm as T. The complexity of algorithm is mainly contributed by the inverse operation of matrix in step 5 and 6, which is $O\big(T(P^3 + N_t^3 L^3)\big)$ flops, where $P = (N_r - 1)L$.

Algorithm 1 Alternate Optimization Algorithm

Input: the center parameter ω_0, the initial signal $\boldsymbol{s}^{(0)}$, a small constant value ϵ and the maximum cycle count M;
Output: $\boldsymbol{s}^{opt}$,$\boldsymbol{t}^{opt}$ and SINR^{opt};

1. with ω_0, calculate $P_{\boldsymbol{A}_0}^{\perp}$ from (5);
2. make decomposition, meeting $P_{\boldsymbol{A}_0}^{\perp} = \boldsymbol{U}\boldsymbol{U}^H$ and $\boldsymbol{U}^H\boldsymbol{U} = \boldsymbol{I}_P$;
3. with $\boldsymbol{U}$, solve the detection model (6);
4. $m \leftarrow 0$, with $\boldsymbol{s}^{(m)}$, get $\text{SINR}^{(m)}$ via (28);
5. with $\boldsymbol{s}^{(m)}$, solve $\boldsymbol{w}^{(m)}$ via (27);
6. with $\boldsymbol{w}^{(m)}$, solve $\boldsymbol{s}^{(m+1)}$ via (31);
7. with $\boldsymbol{s}^{(m+1)}$, obtain $\text{SINR}^{(m+1)}$ via (28);
8. $m = m + 1$, repeat step 5-7, until $|\text{SINR}^{(m)} - \text{SINR}^{(m-1)}|/\text{SINR}^{(m-1)} < \epsilon$ or $m = M$;
9. output the optimal value.

5 Simulation Results

In this Section we will take several simulation examples to make some delights of our above results. The numbers of the transmitting and receiving array elements are set as N_t=4 and N_r=8, and the snap number is L=10. Two signals are located at 10° and 12°, respectively, whose separation is about 34.9% of the Rayleigh limit, which can be calculated by $\pi/(N_rN_t)$. The signal-to-noise rate (SNR) of two signals are all 0 dB, i.e., $\sigma_k^2/\sigma_n^2 = 1$. The the interference-noise-rate (INR) is calculated by $\sigma_{c,k}^2/\sigma_n^2$. The range cell of the k-th interferences is set N=2. We set the maximum count M=1000 or error ϵ=10^{-5} to stop the cycle. We make an comparison with the orthogonal and coherent waveforms, where the latter is linear frequency modulation signals, $\boldsymbol{S}_{coho} \in \mathbb{C}^{N_T \times L}$, as follows

$$\boldsymbol{S}_{coho}(n_t, l) = \sqrt{\frac{p_t}{N_t L}} e^{j\left(N_r(n_t-1)\omega_0 + \pi\left(\frac{l-1}{L}\right)^2\right)}, n_t = 1:N_t, l = 1:L. \tag{32}$$

Example 1: In this example, we set the interferences lie between [30°,40°] with a stride internal angular 1°; hence K=11. We plot the resolution rate versus the transmit energy and INR in Figure 2 and Figure 3, respectively. One can see that, either with fixed INR=20dB and vary the transmit power, or with fixed transmit power P_t=20dB and vary INR, our optimal waveform can outperform the orthogonal and coherent waveforms. Noticing that the coherent waveform exceeds the orthogonal waveform in the low-p_t area but becomes inferior in the high-p_t area. To highlight this, we plot the transceiver beamforming in the Example 2.

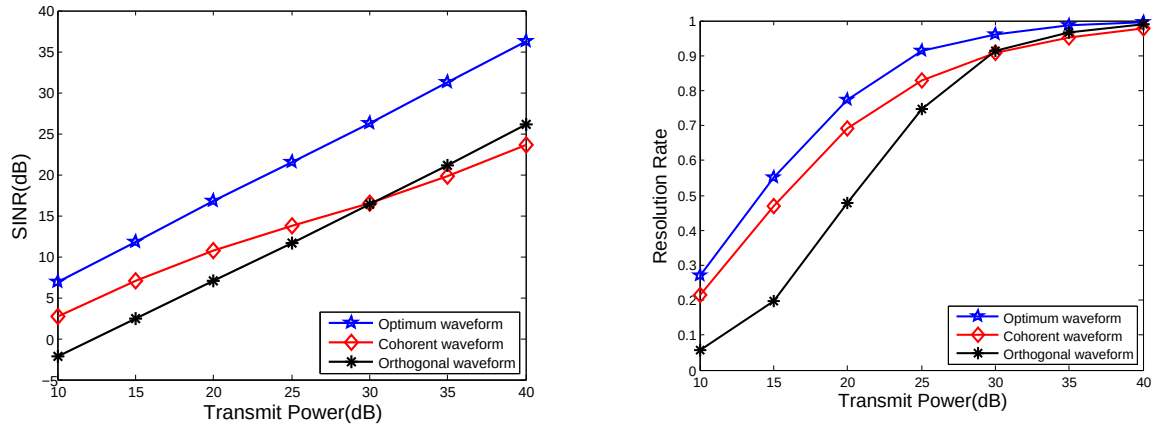

Figure 2 Comparison of different waveforms with INR=20dB.(a) SINR; (b) Resolution Rate.

Example 2: With INR=20dB, we plot the beam pattern for both the transmitting and receiving

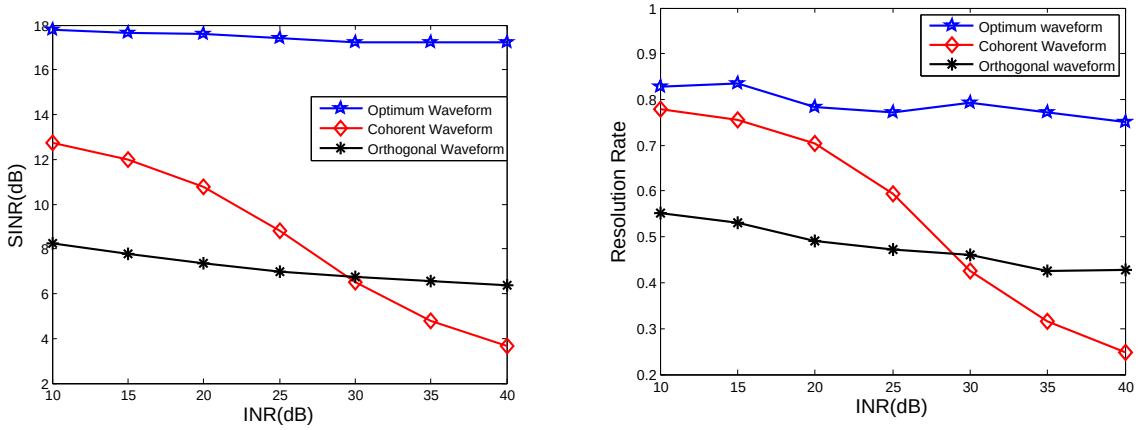

Figure 3 Comparison of different waveforms with P_t=20dB.(a) SINR; (b) Resolution Rate.

beam in Figure 4 for P_t=10dB and P_t=40dB, by the following equation

$$\mathrm{BP} = \frac{|\boldsymbol{w}^H \dot{\boldsymbol{A}}_0^H \boldsymbol{U}\boldsymbol{s}|^2}{N_r N_t |\boldsymbol{w}|^2 |\boldsymbol{s}|^2} = \frac{|\boldsymbol{s}^H \boldsymbol{U}^H \dot{\boldsymbol{A}}_0 \boldsymbol{R}_{nc}^{-1} \dot{\boldsymbol{A}}_0^H \boldsymbol{U}\boldsymbol{s}|^2}{N_r N_t |\boldsymbol{R}_{nc}^{-1} \dot{\boldsymbol{A}}_0^H \boldsymbol{U}\boldsymbol{s}|^2}. \tag{33}$$

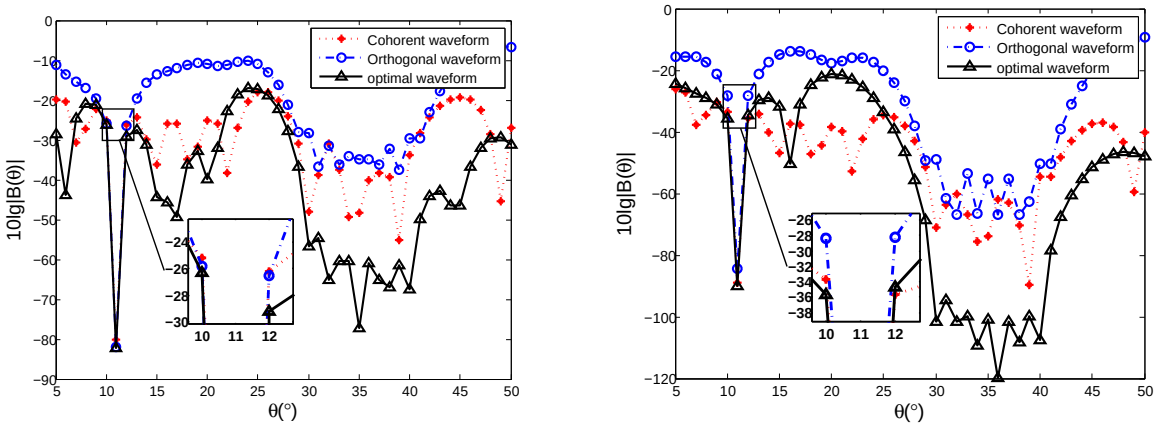

Figure 4 Transceiver beamforming with INR=20dB.(a) P_t=10dB; (b) P_t=40dB.

From Figure 4, one can see that in the high-p_t area (P_t=40dB), the orthogonal waveform has a higher gain at the two target angles than the coherent waveform, so it can achieve a better performance; while in the low-p_t area (P_t=10dB), compared with other waveforms, it has a similar gain at the target angles but a higher gain at the interference angles. In addition, one can see that the all three waveforms have formed a zero-point at the middle angular of two signals, which is caused by the orthogonal projection transformation at the center POI (for this simulation it is 11°).

6 Conclusions

Based on the hypothesis testing theory, we have studied the colocated MIMO waveform design for angular resolution. Our innovations are as follows:

(1) By exploring the Taylor expansion at the known value of angular frequency of two targets and making an orthogonal projection, the original resolution model has been transformed into a detection one. Then, the existing criteria, maximizing SINR criterion and maximizing information entropy, can be implemented.

(2) We have shown the above two criteria to be unified to a universal non-convex model. Then we bring in an alternative optimization algorithm to design the optimal waveform, whose performance outweighs the orthogonal and the coherent waveforms.

Our study provides a new perspective for the MIMO radar waveform design, based on the covariance matrix of the interferences and DOAs of the two targets are known exactly. As this is hard to meet in the reality, some robust design should be considered. In addition, we optimize the waveforms only with the constraint of transmitting energy to highlight our points, some practical conditions such as the constant-modulus and similarity with the given signal waveforms should also be considered.

Acknowledgements This work is supported by the National Key Research and Development Program of China (Grant No. 2016YFA0302102).

References

1 Root WL. Radar Resolution of Closely Spaced Targets. IRE Trans Mil Electron., 1962, MIL-6(2): 197-204
2 Levanon, N. Radar principles. New York: Wiley, 1988:129-143
3 H.Cox, Resolving power and sensitivity to mismatch of optimium array processors. J.Acoust. Soc. America, 1973, 54(3): 771-785
4 Sherman K. C. and Durrani T. S. Resolving Power of Signal Subspace Methods for Finite Data Lengths. International conference on acoustics, speech and signal processing 1985: 1501-1504.
5 Lee HB. The Cramer-Rao Bound on Frequency Estimates of Signals Closely Spaced in Frequency. IEEE Trans Signal Process. 1992,42(6):1569-1572
6 Smith ST. Statistical Resolution Limits and the Complexified Cramer-Rao Bound. IEEE Trans Signal Process, 2005,53(5): 1597-1609
7 Zhi L and Arye N. Statistical Angular Resolution Limit for Point Sources. IEEE Trans Signal Process, 2007,55(11):5521-5527
8 EL Korso MN, Boyer R and Renaux A, et al. On the asymptotic resolvability of two point sources in known subspace interference using a GLRT-based framework. Signal Processing, 2012,92(10):2471-2483
9 El Korso MN, Boyer R, Renaux A, Marcos S. Statistical resolution limit for source localization with clutter interference in a MIMO radar context. IEEE Trans Signal Process., 2012, 60(2):987-992.
10 Zhu W, Tang J and Wan S. Angular Resolution Limit Of Two Closely-spaced Point Sources Based on Information Theoretic Criteria. Int Conf Acoust Speech Signal Process Processing. 2014: 86-90
11 Sun M, Jiang D and Song H, et al. Statistical Resolution Limit Analysis of Two Closely Spaced Signal Sources Using Rao Test. IEEE Access. 2017,5:22013-22022
12 Zhang Y, Zhu W, Tang B, et al. Angular Statistical Resolution Limit of Two Closely-Spaced Point Targets: A GLRT-based Study. in IEEE Access(2018 Early Access).
13 J. Li and P. Stoica. MIMO Radar Signal Processing. Hoboken, NJ, USA: Wiley, 2009.
14 Fuhrmann DR, Member S, Geoffrey San Antonio I, et al. Transmit Beamforming for MIMO Radar Systems using Signal Cross-Correlation. IEEE Trans Aerosp Electron Syst., 2008,44(1):171-186
15 Stoica P, Jian Li, Yao Xie. On Probing Signal Design For MIMO Radar. IEEE Trans Signal Process., 2007,55(8):4151-4161
16 Li J, Stoica P and Zheng X. Signal synthesis and receiver design for MIMO radar imaging. IEEE Trans Signal Process., 2008,56(8):3959-3968
17 Chen CY, Vaidyanathan PP. MIMO radar waveform optimization with prior information of the extended target and clutter. IEEE Trans Signal Process.,2009,57(9):3533-3544
18 Zhu W, Tang J. Robust Design of Transmit Waveform and Receive Filter For Colocated MIMO Radar. Signal Process Lett IEEE. 2015,22(11):2112-2116
19 Tang B, Tang J. Joint Design of Transmit Waveforms and Receive Filters for MIMO Radar Space-Time Adaptive Processing. IEEE Trans Signal Process. 2016,64(18):4707-4722
20 Tang B, Tang J, and Peng Y. MIMO Radar Waveform Design in Colored Noise Based on Information Theory. IEEE Trans. SIGNAL Process. 2010;58(9):4684-4697.
21 Tang B, Naghsh MM, Tang J. Relative Entropy-Based Waveform Design for MIMO Radar Detection in the Presence of Clutter and Interference. IEEE Trans Signal Process., 2015,63(14):3783-3796
22 Yang Y, Blum RS. MIMO Radar Waveform Design Based on Mutual Information and Minimum Mean-Square Error Estimation. Trans Aerosp Electron Syst.,2007,43(1):330-343
23 Zhu Z, Kay S, Raghavan RS. Information-Theoretic Optimal Radar Waveform Design. IEEE Signal Process Lett. 2017;24(3). doi:10.1109/LSP.2017.2655879.
24 Imani S, Ghorashi SA. Transmit Signal and receive filter design in colocated MIMO radar using a transmit weighting matrix. IEEE Signal Process Lett.,2015,22(10):1521-1524
25 R. A. Horn and C. R. Johnson, Matrix Analysis. Cambridge, UK: Cambridge Univ. Press, 1990.